A Journal of the Gesellschaft Deutscher Chemiker

Angewandte International Edition

GDCh

Chemie

www.angewandte.org

Accepted Article

Title: Calixarene-Based Supramolecular AIE Dots with Highly Inhibited Nonradiative Decay and Intersystem Crossing for Ultrasensitive Fluorescence Image-Guided Cancer Surgery

Authors: Chao Chen, Xiang Ni, Han-Wen Tian, Qian Liu, Dong-Sheng Guo, and Dan Ding

To be cited as: *Angew. Chem. Int. Ed.* 10.1002/anie.201916430
Angew. Chem. 10.1002/ange.201916430

Link to VoR: http://dx.doi.org/10.1002/anie.201916430
http://dx.doi.org/10.1002/ange.201916430

WILEY-VCH

10.1002/anie.201916430

WILEY-VCH

Calixarene-Based Supramolecular AIE Dots with Highly Inhibited Nonradiative Decay and Intersystem Crossing for Ultrasensitive Fluorescence Image-Guided Cancer Surgery

Chao Chen[+], Xiang Ni[+], Han-Wen Tian, Qian Liu, Dong-Sheng Guo, and Dan Ding*

Abstract: Molecular motion-associated organic molecules such as aggregation-induced emission luminogens (AIEgens) for disease phototheranostics are attracting increasing attention; however, how to optimally harvest absorbed excitation energy for advanced fluorescence imaging/diagnosis and concurrently avoid unnecessary phototoxicity during bioimaging process is still challenging. To address this issue, herein, we report that the host-guest complexation between calix[5]arene and AIEgen can significantly turn off both the energy dissipation pathways of intersystem crossing and thermal deactivation, enabling the absorbed excitation energy mostly focusing on fluorescence emission. The co-assembly of calix[5]arene amphiphiles and AIEgens affords highly emissive supramolecular AIE nanodots thanks to their interaction extremely restricting the intramolecular motion of AIEgens, which also show negligible cytotoxic reactive oxygen species generation. *In vivo* studies with a peritoneal carcinomatosis-bearing mouse model indicate that such supramolecular AIE dots have rather low *in vivo* side toxicity and can serve as a superior fluorescent bioprobe for ultrasensitive fluorescence image-guided cancer surgery.

Recently, the classes of molecular motion-associated organic molecules including molecular machines, molecular motors and aggregation-induced emission luminogens (AIEgens) are appealing increasing interest in the area of biomedicine, since they provide a new opportunity to achieve optimal theranostic function and efficacy for diseases *via* facilely regulating the molecular motions.[1] Jablonski diagram that elaborates the molecular photophysics can explain the relationship between molecular motion and phototheranostic function/efficacy.[2] According to the Jablonski diagram, after an organic molecule absorbs the excitation light, there are generally three energy dissipation pathways, which are correspondent to different phototheranostic functions: 1) fluorescence emission pathway for fluorescence imaging/diagnosis; 2) intersystem crossing (ISC) to a triplet excited state for phosphorescence afterglow imaging and/or photodynamic therapy through generation of reactive oxygen species (ROS); and 3) thermal deactivation pathway *via* nonradiative decay for photothermal therapy and photoacoustic imaging.[3] As the three dissipation pathways of absorbed excitation energy are always competing, the optimized efficacy of the required phototheranostic function can be realized by suppression of the other pathways. As for molecular motion-associated organic molecules, such photophysical property manipulation is usually determined by molecular motion.

Taking AIEgens with rich intramolecular motion (*e.g.*, rotation, vibration and twisting) units for example, effective restriction of intramolecular motion (RIM) often leads to the promotion of both fluorescence and ROS production by blocking the thermal deactivation route.[4] On the other hand, permitting free intramolecular motions make AIEgens an advanced photothermal conversion material due to the inhibition of radiative and ISC pathways.[5] Based on the aforementioned principle, AIEgens are particularly useful for construction of highly fluorescent nanoparticle bioprobe (termed as AIE dot) due to the formation of intraparticle aggregation astricting the intramolecular motion.[6] Nevertheless, for an overwhelming majority of currently available AIE dots, relatively loose intraparticle packing of AIEgens significantly compromises their fluorescent brightness. Liu, Tang, Zhao, and coworkers reported that crystallization of AIEgens resulted in maximum fluorescence because of the optimally compact packing of AIEgens in crystal minimizing intramolecular motion.[7] However, the crystals even if the nanocrystals that can suspend in water are not suitable for biomedical applications owing to the critical concerns in terms of long-term colloidal stability in biological environments, blood circulation time and uptake efficiency by disease site. Furthermore, in most cases, the red/near-infrared (NIR) emissive AIE dots are able to produce light-activated ROS owing to the electronic donor (D)-acceptor (A) structure usually decreasing the energy gap between the lowest singlet excited state and triplet excited state (ΔE_{ST}),[8] which is decidedly adverse to maximize the emission and causes unnecessary phototoxicity during bioimaging process. Thereby, alternative strategies to build AIE dots with similar restriction degree of intramolecular motion to that in crystal, highly inhibitory ISC and excellent biological accessibility are extremely desirable for advancing the biomedicine field, which however have never been reported yet.

Calixarene, that is a kind of macrocyclic host,[9] has been recently emerged as a promising building block to construct supramolecular nanomedicines/imaging agents,[10] showing the merits of multiple stimuli-responsiveness, numerous modification tunability, and low cytotoxicity.[11] In this work, we first report that the host-guest complexation between calix[5]arene and AIEgen can considerably turn off both the pathways of ISC and thermal deactivation, making utmost absorbed excitation energy used for fluorescence emission. We started with the design and synthesis of a series of AIEgens with D-π-A structure, followed by fabrication of calix[5]arene-based supramolecular AIE dots (S-

[*] Dr. C. Chen,[+] Prof. D. Ding
Tianjin Key Laboratory of Oral and Maxillofacial Function Reconstruction, Tianjin Stomatological Hospital, The Affiliated Stomatological Hospital of Nankai University, Tianjin 300041, China
E-mail: dingd@nankai.edu.cn
Dr. C. Chen,[+] Dr. X. Ni,[+] Prof. D. Ding
State Key Laboratory of Medicinal Chemical Biology, Key Laboratory of Bioactive Materials, Ministry of Education, and College of Life Sciences, Nankai University, Tianjin 300071, China
H. W. Tian, Prof. D. S. Guo
College of Chemistry, State Key Laboratory of Elemento-Organic Chemistry, Key Laboratory of Functional Polymer Materials, Ministry of Education, Nankai University, Tianjin 300071, China
Dr. Q. Liu
Department of Urology, Tianjin First Central Hospital, Tianjin 300192, China
[+] These authors contributed equally to this work.

Supporting information for this article is given via a link at the end of the document.

AIE dots) using carboxylic acid-modified calix[5]arene pentadodecyl ether (CC5A-12C).[12] It is demonstrated that in the presence of CC5A-12C, both the intramolecular motion and ISC transition (ROS generation) of AIEgens can be tremendously restricted, thus leading to ultrabright S-AIE dots in water. Finally, we assessed the *in vivo* toxicity of such S-AIE dots and studied their feasibility and advantage in practical biomedical application in terms of fluorescence image-guided cancer surgery.

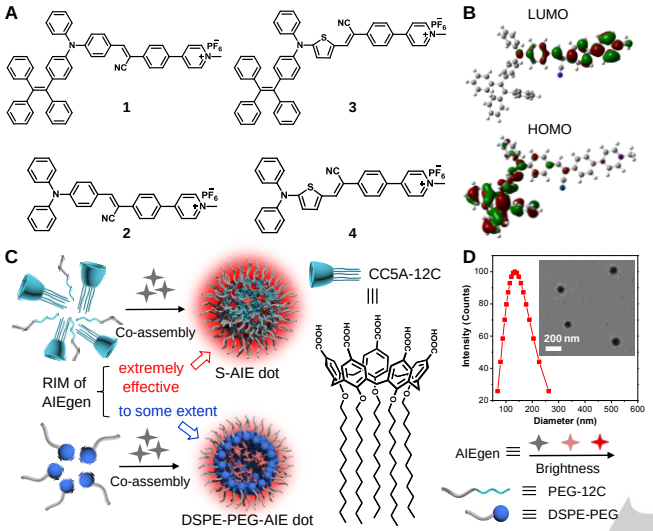

Figure 1. (A) Chemical structures of the AIEgens. (B) The electron density distribution of frontier orbitals of **1**. (C) Schematic of S-AIE dots and DSPE-PEG-AIE dots and chemical structure of CC5A-12C. (D) DLS profile and TEM image (inset) of **1**-loaded S-AIE dots.

Four positively charged AIEgens were synthesized and used to assess the generality of our approach (Figure 1A). Compounds **2**~**4** were synthesized according to the previous literature.[13,14] Figure S1 shows the synthetic route to compound **1** mainly through Knoevenagel condensation and methylation with CH_3I. The intermediates and final compound were characterized by standard spectroscopic techniques (Figure S2-S7). In our molecular design, cyanostilbene/cyanostyrylthiophene acts as the AIE skeleton and π-bridge to build D-π-A structure (pyridinium salt as A). All 4 compounds exhibit prominent AIE effect (Figure S8).[14]

As shown in Figure 1B and Figure S9, density functional theory (DFT) calculations reveal that compared with **2** and **4**, **1** and **3** with crowded TPE unit have much more twisted molecular structures, which are beneficial to reduced intermolecular interactions such as π-π stacking, contributing to stronger AIE activity. The study on electronic structures in the ground state (S_0) at the level of B3LYP/6-31G (d,p) indicates that all the molecules exhibit charge separation characteristic, with the highest occupied molecular orbital (HOMO) electron density majorly distributed on the electron rich segments and the lowest unoccupied molecular orbital (LUMO) electron density mainly distributed on the electron poor moieties. Noteworthy is that for both **1** and **3**, the more effective separations of HOMO-LUMO distribution are helpful in decreasing their ΔE_{ST} and thus boosting ISC and ROS generation efficiency.[8,14]

Next, as illustrated in Figure 1C and Figure S10, pegylated calix[5]arene-based S-AIE dots were prepared by a nanoprecipitation method using CC5A-12C and 4-(dodecyloxy)benzamido-terminated methoxy poly(ethyleneglycol) (PEG-12C) as the matrix of nanocarriers. The AIEgens, **1**~**4**, respectively, were loaded *via* the host-guest complexation between calix[5]arene receptor and each AIEgen. The hydrophilic PEG chains can extend to the water, serving as the protecting outer layer to stabilize the S-AIE dots. The dynamic light scattering (DLS) and transmission electron microscopy (TEM) data depict that the **1**~**4**-loaded S-AIE dots are all spherical in shape with similar mean hydrodynamic diameters of ~150 nm (Figure 1D and Figure S11).

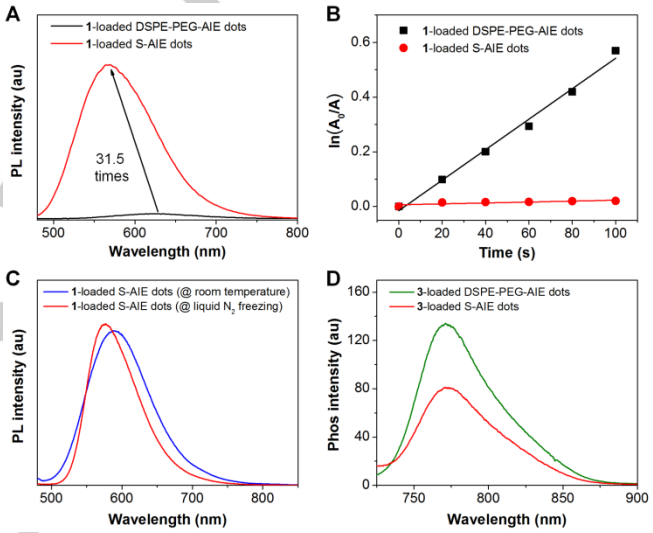

Figure 2. (A) Photoluminescence (PL) spectra of **1**-loaded S-AIE dots and DSPE-PEG-AIE dots in water (λ_{ex}: 445 nm). (B) Plot of $\ln(A_0/A)$ against light irradiation time. A_0 and A represent the ABDA absorbance at 378 nm without and with exposure to white light, respectively. (C) The steady-state PL spectra of **1**-loaded S-AIE dots at room temperature and frozen in liquid nitrogen. (D) The phosphorescence (Phos) spectra, acquired after 10 ms delay, of **3**-loaded DSPE-PEG-AIE dots and S-AIE dots frozen in liquid nitrogen.

The photophysical properties of the as-prepared S-AIE dots were investigated. As a positive control, the most widely used AIE dot doping matrix, 1,2-distearoyl-sn-glycero-3-phosphoethanolamine-*N*-[methoxy(polyethylene glycol)-2000] (DSPE-PEG)[4,6] were also employed to formulate each AIEgen into DSPE-PEG-AIE dots (Figure 1C). The absorption spectra as displayed in Figure S12 indicate that the **1**~**4**-loaded S-AIE dots have an absorption maximum at 442, 440, 478, and 462 nm, respectively, whereas the **1**~**4**-loaded DSPE-PEG-AIE dots show an around 10 nm red-shifted absorption when compared with each corresponding S-AIE dots. Figure S13 displays the emission spectra of **1**~**4**-loaded S-AIE dots in water, respectively, at different mass ratios of CC5A-12C to each AIEgen. When compared with each AIEgen itself in water (mass ratio = 0:1), the fluorescence intensity significantly increases with the increase of CC5A-12C amount, which nearly reaches to the plateau at mass

ratio = 9:1. As shown in Figure 2A and Figure S14, at the same experimental condition, the maximum fluorescent intensities of **1**~**4**-loaded S-AIE dots in aqueous solution are ~31.5, ~19.3, ~10.6, and ~12.5 times higher than the corresponding **1**~**4**-loaded DSPE-PEG-AIE dots, respectively, accompanied with obvious blueshifts of emission peaks. These results reveal that the host-guest complexation can largely boost the emission (mainly ranging from 500 to 750 nm) of AIEgens. As a consequence, using 4-(dicyanomethylene)-2-methyl-6-(*p*-dimethylaminostyryl)-4*H*-pyran in methanol (quantum yield (QY) = 0.43) as the standard, the photoluminescence (PL) QYs of **1**~**4**-loaded S-AIE dots in aqueous solution are determined to be 0.72, 0.50, 0.23, and 0.16, respectively. To our knowledge, QY of 0.72 in water represents one of the highest values among various red-fluorescent materials.[6,15]

The ROS generation capacities of **1**~**4**-loaded S-AIE dots and DSPE-PEG-AIE dots in aqueous media were studied and compared, as all of them are not phosphorescent at room temperature. Using 9,10-anthracenediyl-bis(methylene) dimalonic acid (ABDA) as the ROS indicator,[14] it is found that CC5A-12C greatly diminishes the light-activated ROS generation abilities of all 4 AIEgens (Figure 2B and Figure S15). For instance, upon white light irradiation, the ABDA decomposition rate constant for **1**-loaded DSPE-PEG-AIE dots is as high as 0.00557 s^{-1}, determined by the slope of the plot in Figure 2B, while such constant for **1**-loaded S-AIE dots is negligible and close to zero. This result suggests that the host-guest complexation between calix[5]arene and AIEgen would significantly suppress the ISC pathway.

To deeply understand the difference in photophysical property between S-AIE dots and DSPE-PEG-AIE dots, fluorescence anisotropy study was firstly performed with the widely used 1,6-diphenyl-1,3,5-hexatriene (DPH) as the probe. The DPH emission is polarized upon the excitation with polarized light. The extent of polarization depends on the orientation of DPH relative to the direction of the polarized excitation, while the rotational motion of DPH causes depolarization. The more viscous the microenvironment is, the larger restriction extent of the rotational motion will be provided, which leads to a less depolarization and thus a higher fluorescence anisotropy value.[16] It is found that for **1**-loaded DSPE-PEG-AIE dots, the fluorescence anisotropy value of DPH is determined to be 0.219. Interestingly, for **1**-loaded S-AIE dots, the fluorescence anisotropy value reaches up to 0.392, which is nearly equal to the intrinsic anisotropy of DPH (0.395).[17] The extremely high polarization of DPH fluorescence indicates that the intramolecular motion of **1** in the presence of CC5A-12C can be thoroughly restricted. Furthermore, the steady-state PL spectra of **1**-loaded S-AIE dots at room temperature and frozen in liquid nitrogen were measured. As displayed in Figure 2C, although the freezing effect of liquid nitrogen is able to further restrict the intramolecular motion of AIEgen in theory, the maximum fluorescence intensity is hardly changed before and after decreasing the temperature of AIE dot solution, implying that the intramolecular motion of **1** has already been suppressed effectively by CC5A-12C even at room temperature. In addition, the emission peaks of S-AIE dots are significantly blue-shifted when compared with those of DSPE-PEG-AIE dots (Figure 2A and Figure S14), revealing the effectively restricted intramolecular twisting between D and A inhibiting twisted intramolecular charge transfer (TICT) process. We next optimized the structures of **1** and CC5A-12C in the S_0 state, respectively, at the ωB97xD/6-31G(d,p) level in Gaussian 09 package, which indicate that **1** locates on the outside of calix[5]arene while **1** and CC5A-12C align through a quasi-antiparallel mode. The distance between **1** and CC5A-12C is quite close which helps rigidify the intramolecular motion of **1** (Figure S16). These results together reasonably verify the extremely efficient RIM in S-AIE dots, leading to vitally inhibitory thermal deactivation pathway.

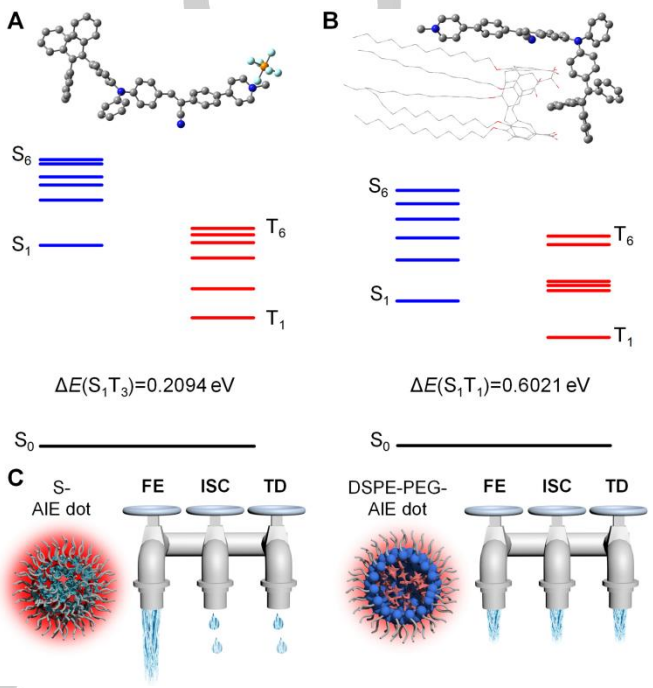

Figure 3. Optimized molecular structures and calculated energy diagrams of (A) **1** and (B) "**1**+CC5A-12C" complex. (C) Schematic of 3 dissipation pathways of the absorbed excitation energy for different AIE dots, which are likened to 3 water taps. FE: fluorescence emission; TD: thermal deactivation.

Besides ROS generation, the influence of CC5A-12C on ISC transition was also studied through measurement of low temperature phosphorescence of both S-AIE dots and DSPE-PEG-AIE dots. As depicted in Figure 2D and Figure S17, **3**- and **4**-loaded AIE dots possess low temperature phosphorescence when frozen in liquid nitrogen. Noteworthy is that the phosphorescence intensities of S-AIE dots are much lower than those of DSPE-PEG-AIE dots, indicating the reduced ISC transition by CC5A-12C. Since ΔE_{ST} correlates closely with the ISC process,[8] we calculated the energy levels of singlet and triplet excited states based on the structures at $S_{0,min}$ of **1** and "**1**+CC5A-12C" complex. The results in Figure 3A,B demonstrate that the ΔE_{ST} of the complex is much larger than that of **1** itself. The increased ΔE_{ST} value is probably attributed to the structure rigidification of **1** by the multiple intermolecular interactions between **1** and CC5A-12C. As a result, if we liken the three dissipation pathways of the absorbed excitation energy to three

water taps, the host-guest complexation between calix[5]arene and AIEgen significantly turns off the taps of ISC and thermal deactivation, enabling the "water" (absorbed excitation energy) mostly flow out as the fluorescence (Figure 3C).

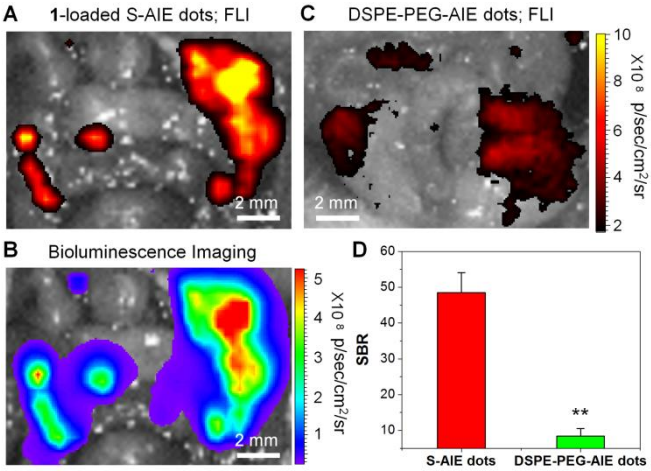

Figure 4. (A) Typical fluorescence imaging (FLI) and (B) bioluminescence imaging of the intraperitoneal tumor nodules from mice after intravenous injection of **1**-loaded S-AIE dots for 24 h. (C) Typical FLI of **1**-loaded DSPE-PEG-AIE dot-treated mice at 24 h post-injection. (D) SBR based on the FLI in (A) and (C). ** $P < 0.01$, in comparison between two types of AIE dots.

The **1**-loaded S-AIE dots were selected for the next biomedical application due to the ultrahigh PL QY. After validating that the S-AIE dots have rather low cytotoxicity and *in vivo* side toxicity (Figure S18-S21), their application in fluorescence image-guided cancer surgery (FIGCS) was performed. Very recently, FIGCS has received great attention and applied in the clinic, as it can essentially help the surgeon improve the outcome of tumor removal operation.[18] Development of bright fluorescent probes with rather high signal-to-background ratio (SBR) is in urgent pursuit.[19] To estimate the utility of our S-AIE dots in FIGCS, a peritoneal carcinomatosis-bearing mouse model was established by intraperitoneal injection of luciferase-expressed murine 4T1 cancer cells. Such tumor-bearing mouse model has two characters: 1) there are many tumor nodules including tiny ones with diameters < 1 mm dispersed in the abdominal cavity; and 2) the tumor nodules/cells can emit bioluminescence upon injection of D-luciferin by virtue of the interaction between luciferase and D-luciferin, allowing for precise tumor localization.

The tumor-bearing mice were intravenously injected with **1**-loaded S-AIE dots (100 μL, 0.25 mg mL^{-1} based on **1**), which was followed by opening the mouse abdomen at 24 h post-administration. The mice were then imaged during operation using IVIS® *in vivo* fluorescence imaging system. As displayed in Figure 4A and Figure S22, the S-AIE dots are capable of significantly accumulating into and lighting up intraperitoneal tumor nodules through remarkable enhanced permeability and retention (EPR) effect,[20] confirmed by the good colocalization with tumor bioluminescence post D-luciferin injection (Figure 4B) and the hematoxylin and eosin (H&E) histological analysis (Figure S23). Encouragingly, the SBR[21] (tumor-to-surrounding normal intestine) for S-AIE dot-treated mice is determined to be 48.5 ± 5.6, which represents the highest among various fluorescent probes for FIGCS *via* intravenous injection, to the best of our knowledge. In comparison, another group of tumor-bearing mice were intravenously injected with 100 μL of **1**-loaded DSPE-PEG-AIE dots with the same concentration of **1** as that of S-AIE dots. Although DSPE-PEG-AIE dots are also able to accurately outline the intraperitoneal metastatic tumors by fluorescence, the SBR value (8.4 ± 2.1) is far lower than that achieved by S-AIE dots (Figure 4D). Furthermore, the data in Figure S24 and S25 prove that the S-AIE dots give superb performance in FIGCS during surgery, considerably improving the outcome of tumor removal operation.

In summary, we have introduced an alternative class of fluorescent probes with ultrahigh brightness by taking advantage of AIE property and host-guest complexation between calix[5]arene and AIEgen. When compared with currently available fluorescent bioprobes including AIEgen-based ones, the uniqueness of calix[5]arene-based S-AIE dots includes: 1) providing one of the very limited examples of AIEgen-based bioprobes with the intramolecular motion of AIEgen close to complete restriction; 2) both the pathways of ISC and thermal deactivation are concurrently inhibited by calix[5]arene, leading to the absorbed excitation energy mostly focusing on fluorescence emission. This is not achievable by previous reported AIEgen-based probes; 3) as a result, the **1**-loaded S-AIE dots have an ultrahigh PL QY of 0.72, which is one of the highest values among various red-fluorescent materials in water; and 4) the **1**-loaded S-AIE dots can realize *in vivo* SBR (tumor-to-normal tissue) of ~48.5, which represents the highest among various fluorescent probes for FIGCS *via* intravenous injection. Moreover, the compromised ROS production of S-AIE dots is beneficial to avoid unnecessary phototoxicity during bioimaging. Thereby, this study demonstrates that calixarene is an ideal platform to develop advanced AIE bioprobes.

Acknowledgements

This work was supported by the NSFC (51873092 and 51873090), and the Fundamental Research Funds for the Central Universities, Nankai University.

Keywords: aggregation-induced emission • calixarene • supramolecular nanoparticle • photophysical property • fluorescence image-guided cancer surgery

[1] a) S. Kassem, T. van Leeuwen, A. S. Lubbe, M. R. Wilson, B. L. Feringa, D. A. Leigh, *Chem. Soc. Rev.* **2017**, *46*, 2592-2621; b) S. Erbas-Cakmak, D. A. Leigh, C. T. McTernan, A. L. Nussbaumer, *Chem. Rev.* **2015**, *115*, 10081-10206; c) J. P. Sauvage, *Angew. Chem. Int. Ed.* **2017**, *56*, 11080-11093; d) Z. Zhao, C. Chen, W. Wu, F. Wang, L. Du, X. Zhang, Y. Xiong, X. He, Y. Cai, R. T. K. Kwok, J. W. Y. Lam, X. Gao, P. Sun, D. L. Phillips, D. Ding, B. Z. Tang, *Nat. Commun.* **2019**, *10*, 768.

[2] H. Qian, M. E. Cousins, E. H. Horak, A. Wakefield, M. D. Liptak, I. Aprahamian, *Nat. Chem.* **2017**, *9*, 83-87.

[3] a) K. Pu, J. Mei, J. V. Jokerst, G. Hong, A. L. Antaris, N. Chattopadhyay, A. J. Shuhendler, T. Kurosawa, Y. Zhou, S. S. Gambhir, Z. Bao, J. Rao,

Adv. Mater. **2015**, *27*, 5184-5190; b) K. K. Ng, G. Zheng, *Chem. Rev.* **2015**, *115*, 11012-11042; c) J. Qi, C. Chen, X. Zhang, X. Hu, S. Ji, R. T. K. Kwok, J. W. Y. Lam, D. Ding, B. Z. Tang, *Nat. Commun.* **2019**, *9*, 1848; d) Y. Jiang, K. Pu, *Acc. Chem. Res.* **2018**, *51*, 1840-1849.

[4] a) J. Qi, C. Chen, D. Ding, B. Z. Tang, *Adv. Healthcare Mater.* **2018**, *7*, 1800477; b) F. Hu, S. Xu, B. Liu, *Adv. Mater.* **2018**, *30*, 1801350; c) C. Chen, H. Ou, R. Liu, D. Ding, *Adv. Mater.* **2019**, *31*, 1806331.

[5] a) S. Liu, X. Zhou, H. Zhang, H. Ou, J. W. Y. Lam, Y. Liu, L. Shi, D. Ding, B. Z. Tang, *J. Am. Chem. Soc.* **2019**, *141*, 5359-5368; b) H. Ou, S. Dai, R. Liu, D. Ding, *Sci. China Chem.* **2019**, *62*, 929-932.

[6] G. Feng, B. Liu, *Acc. Chem. Res.* **2018**, *51*, 1404-1414.

[7] S. M. A. Fateminia, Z. Wang, C. C. Goh, P. N. Manghnani, W. Wu, D. Mao, L. G. Ng, Z. Zhao, B. Z. Tang, B. Liu, *Adv. Mater.* **2017**, *29*, 1604100.

[8] S. Xu, Y. Yuan, X. Cai, C. J. Zhang, F. Hu, J. Liang, G. Zhang, D. Zhang, B. Liu, *Chem. Sci.* **2015**, *6*, 5824-5830.

[9] a) R. Kumar, A. Sharma, H. Singh, P. Suating, H. S. Kim, K. Sunwoo, I. Shim, B. C. Gibb, J. S. Kim, *Chem. Rev.* **2019**, *119*, 9657-9721; b) B. Han, X. Wang, Y. Gao, M. Bai, *Chem. Eur. J.* **2016**, *22*, 16037-16041; c) B. P. Jiang, D. S. Guo, Y. C. Liu, K. P. Wang, Y. Liu, *ACS Nano* **2014**, *8*, 1609-1618; d) H. Shigemitsu, I. Hamachi, *Chem. Eur. J.* **2015**, *10*, 2026-2038; e) C. Zhang, Z. Wang, S. Song, X. Meng, Y. S. Zheng, X. L. Yang, H. B. Xu, *J. Org. Chem.* **2015**, *79*, 2729-2732.

[10] a) J. Mo, P. K. Eggers, Z. Yuan, C. L. Raston, L. Y. Lim, *Sci. Rep.* **2016**, *6*, 23489; b) J. S. Kim, D. T. Quang, *Chem. Rev.* **2007**, *107*, 3780-3799; c) X. M. Chen, Y. Chen, Q. Yu, B. H. Gu, Y. Liu, *Angew. Chem. Int. Ed.* **2018**, *57*, 12519-12523; d) D. S. Guo, V. D. Uzunova, X. Su, Y. Liu, W. M. Nau, *Chem. Sci.* **2011**, *2*, 1722-1734; e) M. A. Beatty, J. Borges-Gonzálẹz, N. J. Sinclair, A. T. Pye, F. Hof, *J. Am. Chem. Soc.* **2018**, *140*, 3500-3504; f) V. Bagnacani, V. Franceschi, M. Bassi, M. Lomazzi, G. Donofrio, F. Sansone, A. Casnati, R. Ungaro, *Nat. Commun.* **2013**, *4*, 1721; g) J. Zhou, B. Hua, L. Shao, H. Feng, G. Yu, *Chem. Commun.* **2016**, *52*, 5749-5752.

[11] a) S. B. Nimse, T. Kim, *Chem. Soc. Rev.* **2013**, *42*, 366-386; b) Y. Zhou, H. Li, Y. W. Yang, *Chinese Chem. Lett.* **2015**, *26*, 825-828; c) M. A. Beatty, A. J. Selinger, Y. Li, F. Hof, *J. Am. Chem. Soc.* **2019**, *141*, 16763-16771; d) A. Hennig, H. Bakirci, W. M. Nau, *Nat. Methods.* **2007**, *4*, 629-632; e) F. Zhu, G. Yang, M. K. Dhinakaran, R. Wang, M. Song, H. Li, *Chem. Commun.* **2019**, *55*, 12833-12836; f) X. T. Lou, Y. W. Yang, *Adv. Optical Mater.* **2018**, *6*, 1800668; g) H. Wang, X. Ji, Z. Li, F. Huang, *Adv. Mater.* **2017**, *29*, 1606117.

[12] Z. Xu, S. Peng, Y. Y. Wang, J. K. Zhang, A. I. Lazar, D. S. Guo, *Adv. Mater.* **2016**, *28*, 7666-7671.

[13] C. Y. Y. Yu, H. Xu, S. Ji, R. T. K. Kwok, J. W. Y. Lam, X. Li, S. Krishnan, D. Ding, B. Z. Tang, *Adv. Mater.* **2017**, *29*, 1606167.

[14] C. Chen, X. Ni, S. Jia, Y. Liang, X. Wu, D. Kong, D. Ding, *Adv. Mater.* **2019**, *31*, 1904914.

[15] C. Wu, S. J. Hansen, Q. Hou, J. Yu, M. Zeigler, Y. Jin, D. R. Burnham, J. D. McNeill, J. M. Olson, D. T. Chiu, *Angew. Chem. Int. Ed.* **2011**, *50*, 3430-3434.

[16] a) B. R. Lentz, *Chem. Phys. Lipids* **1993**, *64*, 99-116; b) X. Zhang, L. E. Kirsch, *Pharm. Dev. Technol.* **2004**, *9*, 219-227.

[17] J. R. Lakowicz, F. G. Prendergast, D. Hogen, *Biochemistry* **1979**, *18*, 508-519.

[18] A. L. Vahrmeijer, M. Hutteman, J. R. van der Vorst, C. J. H. van de Velde, J. V. Frangioni, *Nat. Rev. Clin. Oncol.* **2013**, *10*, 507-518.

[19] a) T. Zhao, G. Huang, Y. Li, S. Yang, S. Ramezani, Z. Lin, Y. Wang, X. Ma, Z. Zeng, M. Luo, E. de Boer, X. J. Xie, J. Thibodeaux, R. A. Brekken, X. Sun, B. D. Sumer, J. Gao, *Nat. Biomed. Eng.* **2017**, *1*, 0006; b) Y. Sun, M. Ding, X. Zeng, Y. Xiao, H. Wu, H. Zhou, B. Ding, C. Qu, W. Hou, A. Er-bu, Y. Zhang, Z. Cheng, X. Hong, *Chem. Sci.* **2017**, *8*, 3489-3493; c) P. Wang, Y. Fan, L. Lu, L. Liu, L. Fan, M. Zhao, Y. Xie, C. Xu, F. Zhang, *Nat. Commun.* **2018**, *9*, 2898; d) K. Shou, Y. Tang, H. Chen, S. Chen, L. Zhang, A. Zhang, Q. Fan, A. Yu, Z. Cheng, *Chem. Sci.* **2018**, *9*, 3105-3110.

[20] X. Zheng, H. Mao, D. Huo, W. Wu, B. Liu, X. Jiang, *Nat. Biomed. Eng.* **2017**, *1*, 0057.

[21] Q. Miao, C. Xie, X. Zhen, Y. Lyu, H. Duan, X. Liu, J. V. Jokerst, K. Pu, *Nat. Biotechnol.* **2017**, *35*, 1102-1110.

10.1002/anie.201916430

WILEY-VCH

Entry for the Table of Contents

COMMUNICATION

A series of calix[5]arene -based supramolecular AIE nandots were synthesized with rather high quantum yields in water by virtue of the host-guest complexation making the absorbed excitation energy mostly focusing on fluorescence emission, which thus realized ultrahigh signal-to-background ratio in fluorescence image-guided cancer surgery.

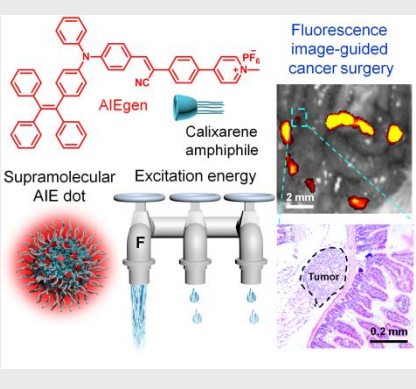

*Chao Chen[+], Xiang Ni[+], Han-Wen Tian, Qian Liu, Dong-Sheng Guo, and Dan Ding**

Page No. – Page No.

Calixarene-Based Supramolecular AIE Dots with Highly Inhibited Nonradiative Decay and Intersystem Crossing for Ultrasensitive Fluorescence Image-Guided Cancer Surgery